Nanoscale

Accepted Manuscript

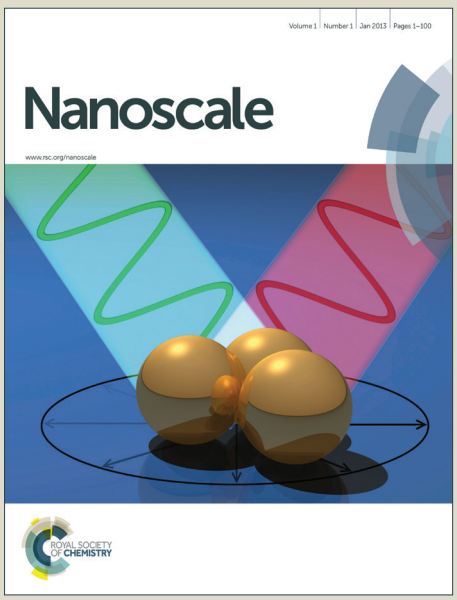

This is an *Accepted Manuscript*, which has been through the Royal Society of Chemistry peer review process and has been accepted for publication.

Accepted Manuscripts are published online shortly after acceptance, before technical editing, formatting and proof reading. Using this free service, authors can make their results available to the community, in citable form, before we publish the edited article. We will replace this *Accepted Manuscript* with the edited and formatted *Advance Article* as soon as it is available.

You can find more information about *Accepted Manuscripts* in the Information for Authors.

Please note that technical editing may introduce minor changes to the text and/or graphics, which may alter content. The journal's standard Terms & Conditions and the Ethical guidelines still apply. In no event shall the Royal Society of Chemistry be held responsible for any errors or omissions in this *Accepted Manuscript* or any consequences arising from the use of any information it contains.

ROYAL SOCIETY OF CHEMISTRY

www.rsc.org/nanoscale

Shape-directional growth of Pt and Pd nanoparticles†

G. Jeremy Leong, [a,b,‡] Abbas Ebnonnasir,[c,d,‡] Maxwell C. Schulze,[a] Matthew B Strand,[a] Chilan Ngo,[d] David Maloney,[a] Sarah L. Frisco,[a] Huyen N. Dinh,[b] Bryan Pivovar,[b] George H. Gilmer,[c] Suneel Kodambaka,[d] Cristian V. Ciobanu,[c] and Ryan M. Richards[a,*]

[a]Department of Chemistry and Geochemistry, Colorado School of Mines, Golden, Colorado 80401, USA. Email: rrichard@mines.edu; Tel: +1 303 273 3612

[b]Chemical and Materials Science Center, National Renewable Energy Laboratory, Golden, Colorado 80401, USA.

[c]Department of Mechanical Engineering, Colorado School of Mines, Golden, Colorado 80401, USA.

[d]Department of Materials Science and Engineering, University of California Los Angeles, Los Angeles, California 90095, USA

†Electronic Supplementary Information (ESI) available: TEM images of platinum nanoparticles synthesized in the presence of different directing agents.

‡These authors contributed equally to this work

Nanoscale Accepted Manuscript

Abstract

The design and synthesis of shape-directed nanoscale noble metal particles have attracted much attention due to their enhanced catalytic properties and the opportunities to study fundamental aspects of nanoscale systems. As such, numerous methods have been developed to synthesize crystals with tunable shapes, sizes, and facets by adding foreign species that promote or restrict growth on specific sites. Many hypotheses regarding how and why certain species direct growth have been put forward, however there has been no consensus on a unifying mechanism of nanocrystal growth. Herein, we develop and demonstrate the capabilities of a mathematical growth model for predicting metal nanoparticle shapes by studying a well known procedure that employs $AgNO_3$ to produce {111} faceted Pt nanocrystals. The insight gained about the role of auxiliary species is then utilized to predict the shape of Pd nanocrystals and to corroborate other shape-directing syntheses reported in literature. The fundamental understanding obtained herein by combining modeling with experimentation is a step toward computationally guided syntheses and, in principle, applicable to predictive design of the growth of crystalline solids at all length scales (nano to bulk).

Keywords: wet chemical reduction; nanoparticle; shape-direction; materials design; palladium; platinum

Introduction

Morphological direction of nanoscale noble metals such as platinum (Pt) and palladium (Pd) are receiving increased interest due to potential facet-dependent enhanced catalytic properties, which can be obtained by directed syntheses of nanocrystals with specific shapes.[1-4] The importance of specific surface faceting with respect to catalytic processes has been explored *via* computational modeling and studies of bulk single-crystal surfaces in ultra-high vacuum.[5-8] Such studies have provided the foundation toward an understanding of catalytic activity and selectivity. Due to the emerging field of shaped nanoparticle (NP) synthesis, results of early surface science studies can now be tested at the nanoscale at elevated temperatures and pressures typical of the working conditions found in industrial processes. Pt is used in hydrogenation reactions,[1,9-13] carbon

Nanoscale Accepted Manuscript

monoxide oxidation,[14-16] and oxygen reduction reactions (ORR),[7,9,17-19] while Pd is used for similar reactions,[11,20-26] and is notable for its carbon-carbon coupling reactions.[27-30]

Numerous physical and chemical properties are dramatically influenced by size, shape, and composition at the nanoscale. Increased catalytic efficiency has been reported for systems possessing specific surface facets[31] with different binding energies, atomic packing, and coordination from step edges and defects; all of which influence both catalytic activity[7,32-34] and selectivity.[9,12,35] Syntheses of novel shapes including cubes, cuboctahedra, multipods, nanorods, nanostars, octahedra, spheres, tetrahedra, icosahedra, dodecahedra, plates, and porous structures have recently been reported however fundamental studies of nanoscale surface facets provide opportunities for further development.[1-234,9,36-41] While most studies have leveraged serendipitous experimental discovery of the different crystal morphologies, relatively few have focused on understanding morphology direction mechanisms. Amongst these studies, most focus on twinned-crystal seeds, anisotropic or overgrowth conditions, and seed mediated conditions,[1,3,4,42,43] dealing with either capping agents or auxiliary directing species that bind to specific facets, changing surface energies and relative attachment rates. Shape direction can also occur in the presence of a hard template such as mesoporous silica networks, where deposition of platinum within the mesopores of the template results in the formation of nanostructures that are inverted replicas of the template.[38-40] A materials design approach where mechanistic understanding is used in computational modeling and data sharing to direct experimental work has the potential to increase the development rate of new materials.[44]

In this article, the mechanism of directing NP shape was investigated through a continuous feedback loop of experimentation coupled with computational modeling by utilizing a well-known, robust procedure for synthesizing shaped Pt NPs with high yields. The method utilizes a wet chemical reduction (WCR) reaction with polyvinylpyrrolidone (PVP) as a capping agent and silver nitrate ($AgNO_3$) as a directing agent.[45,46] Cubic, cuboctahedral, and octahedral NPs bounded by {001} and {111} facets can be produced for face-centered cubic (fcc) metal since {111} and {001} are two of the three lowest energy surfaces in fcc crystals.[36] It is proposed that silver influences the direction of growth, though nitrate (NO_3) has also been shown to direct growth of Pt in a different synthetic system using $NaNO_3$.[47] It has been reported that silver can

Nanoscale Accepted Manuscript

exist as a number of ions, clusters, or zero-valent species in ethylene glycol,[48] and we will refer to those species in general as Ag. Herein, we experimentally identify if Ag or NO_3 is responsible for directing NP morphology in this system by studying both the intermediate and final products as a function of growth time. We develop an experimentally-verifiable continuum model for the directed growth of faceted NPs and use it to not only explain but also predict and guide the observed Pt and Pd NP morphologies. In doing so, we demonstrate the powerful synergy of coupling computational modeling with materials synthesis thus opening up the potential to design, rather than discover by trial-and-error experimentation, new and improved catalysts of the future.

Results and Discussion

Ag-directed growth of Pt NPs *via* WCR Experimentation

Ag was reported to influence Pt NP shape in a polyol WCR synthesis by preferentially affecting growth onto different facets,[1,45] while NO_3 was reported to direct Pt NP shape in a similar synthetic system where non-reflux temperatures (160 ˚C) allowed the NO_3 to slow reduction kinetics, resulting in overgrowth conditions.[1,47] To distinguish between the shape directing roles of Ag and NO_3 in the synthesis outlined by Yang and co-workers,[45] we utilized the reflux procedure outlined in the methods section and systematically varied the auxiliary directing agents across broad concentration ranges to isolate and identify the species responsible for shape-direction in this system. Only those salts soluble in ethylene glycol, including Ag halides and sulfates and a variety of alkali, alkali-earth, and transition-metal nitrates were tested. For comparison, control experiments were conducted using corresponding salts with neither Ag nor NO_3. Additionally, mixtures of $AgNO_3$ and $NaNO_3$ were used as the directing agents to test the concentration dependency of the refluxing system on both Ag and NO_3 simultaneously. The mixture concentrations were chosen to have Ag and NO_3 species at different concentrations, but at similar concentrations of $AgNO_3$ reported to yield the morphologies shown in Figure 1.[45]

Nanoscale Accepted Manuscript

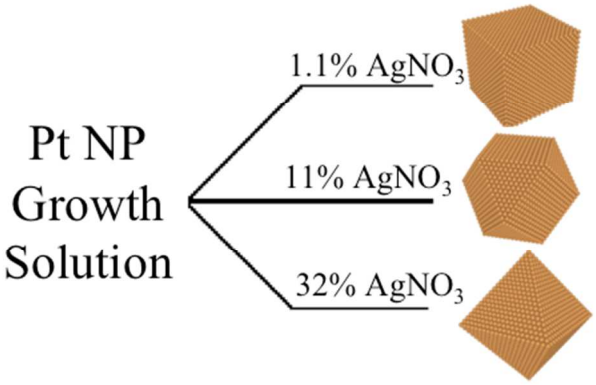

Figure 1. The shapes of the Pt NPs are dependent on the concentration of $AgNO_3$ in this system. Ag/Pt: 1.1 mol%, 11 mol%, and 32 mol% $AgNO_3$ producing relatively monodispersed in size and shape cubes, cuboctahedra, and octahedra, respectively.[45]

A mixture of 1.1 mol% $AgNO_3$ and 9.9 mol% $NaNO_3$ produced Pt NPs with cubic morphology (Figure 2A,D) as dictated from the 1.1 mol% Ag rather than cuboctahedral morphology (Figure 2B,E), which would be expected if direction were obtained from the 11 mol% NO_3. Similarly, a mixture of 11 mol% $AgNO_3$ and 21 mol% $NaNO_3$ produced cuboctahedral morphology (Figure 2B,E) as dictated by 11 mol% Ag rather than octahedral morphology (Figure 2C,F) if direction were obtained by 32 mol% NO_3. The collective results indicate that only Ag containing salts resulted in NPs with uniform morphologies for this specific system, and that NO_3 was not influential for direction at the elevated reflux temperatures (see supplementary information). The observation that lower and higher molar ratios of Ag to Pt result in the preponderance of cubic ({001} bound) and octahedral ({111} bound) morphologies, respectively, supports the hypothesis that Ag is indeed responsible for shape-direction by affecting preferential attachment fluxes of Pt atoms to different surfaces during growth, as reported previously.[45] In the following sections, we describe a model that is developed in concert with the experimentally-supported hypothesis that Ag concentration dictates Pt NP morphologies.

Nanoscale Accepted Manuscript

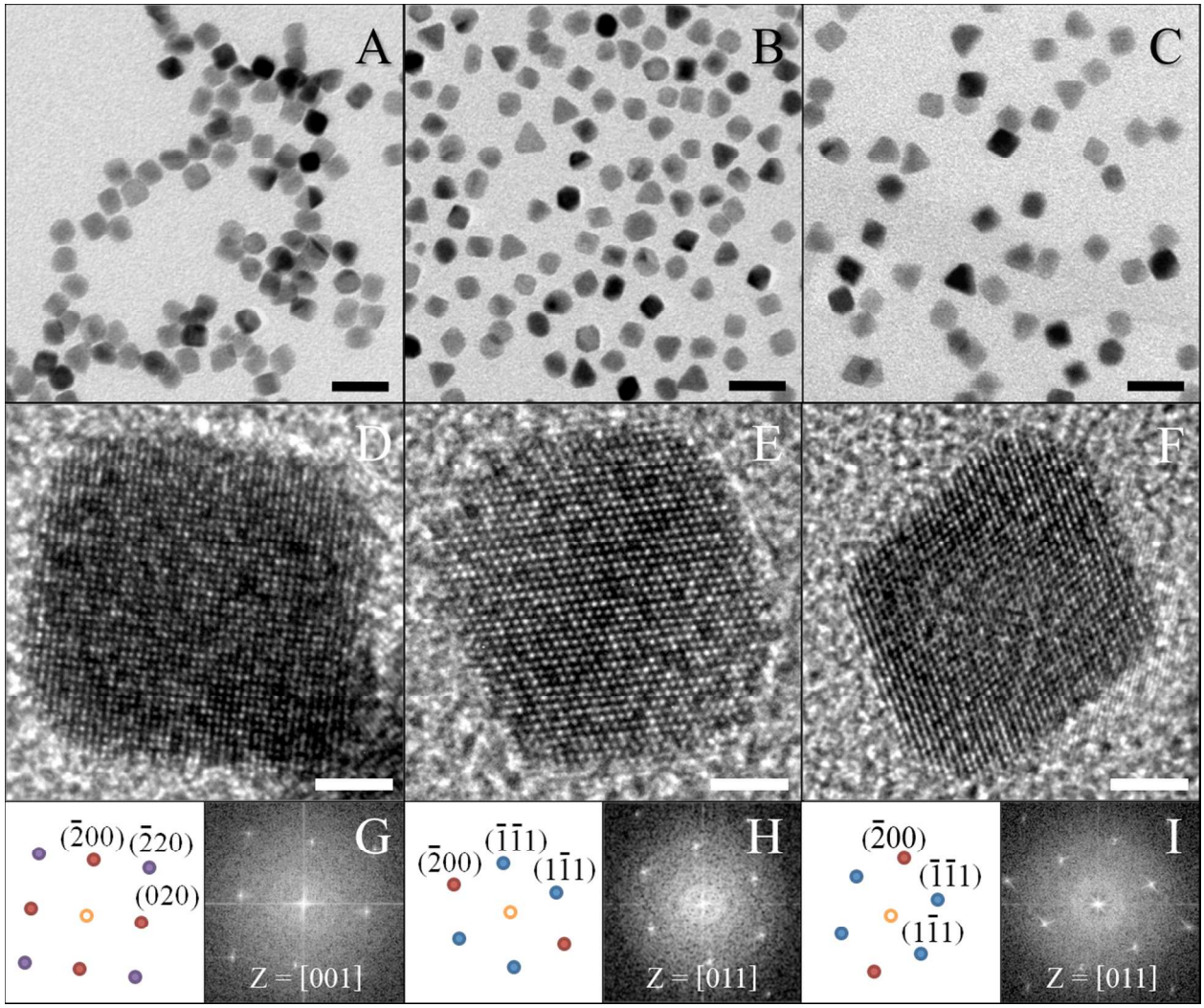

Figure 2. Transmission electron microscopy (TEM) (top images A, B, C) and high-resolution TEM (HRTEM) micrographs (bottom images D, E, F) along with corresponding Fourier transforms and their indexes (G, H, I) of the HRTEM images of shaped Pt NPs resulting from different Ag concentrations in solution during growth. (A,D) Ag/Pt: 1.1 mol% produces cubes with predominantly {001} surface facets, (B,E) Ag/Pt: 11 mol% produces cuboctahedra bounded by {001} and {111} surface facets, and (C,F) Ag/Pt: 32 mol% produces octahedra with {111} surface facets. The scale bars in A-C are 20 nm and in D-F are 2 nm.

Developing Growth Model for NP Shape-Direction

Basis of Growth Model

Most models pertaining to NP shape rely at least in some qualitative manner on the Wulff construction,[49] which relates the surface energies of different facet orientations with the area of those facets: the smaller its surface energy, the closer that facet is to the "center" of the NP, and thus the larger surface area it has. There are potential problems with such an approach, which

Nanoscale Accepted Manuscript

manifest more acutely in the case of growth *via* wet chemical reduction (WCR). The surface energies computed for most metals are performed under vacuum, not in the presence of a solution containing the precursor metal salt and directing agents. Surface energy values in such wet chemical environments are far from those that can be obtained *via* atomic scale calculations in vacuum (embedded atom method,[50] or density functional theory[51,52]). Furthermore, the surface energies and their relative ordering in solution change as a function of the super-saturation of the metal atoms (*e.g.*, by injecting desired levels of precursor salt in solution), thus discussions of the final shapes by using surface energies computed in vacuum and at a fixed value of the chemical potential may be far from reality. These deficiencies prompt us to recall that, on a fundamental level, the Wulff construction gives equilibrium crystal shape under the constraint of constant NP volume, which is not the case here. Our experiments show that to effectively direct the final crystal shape, it is necessary for the complete reaction solution including the directing agent to be present during growth from nucleation to final product. There can exist a narrow time window following nucleation in which the roughly spherical NP does not grow significantly, but suddenly acquires well-defined facets. The very short-lived process can be understood based on the Wulff construction because it occurs at (nearly) constant volume, provided one has the correct surface energies obtained for the specific solution conditions. After a nucleus acquires facets, it grows in the presence of metal precursor salts and directing agents in solution. This is the growth process that we will address here, by employing a model for growth that allows the relative size of the facets to change over time.

Generic model for arbitrary facets during growth

In principle, there exists a kinematic Wulff construction designed to give the shape of a particle during growth, which requires knowledge of the growth velocity $\mathbf{V}(\mathbf{n})$ as a continuous function of the normal at the surface $\mathbf{n}$.[53] In our model, we will deal with discrete surface orientations and consider the effect of the directing agent (*e.g.* $AgNO_3$). Here, we consider two low-index orientations of the surface, for clarity, {001} and {111}, however, the arguments and calculations can be carried out in the same manner for any two intersecting facets of the NP. Their growth rates are different because of the varying attachment rates of Pt (main metal) and Ag (directing agent) at the two surface orientations considered. It has been hypothesized that Ag can hinder the attachment of Pt on the {111} orientation, but not on other orientations or at least

Nanoscale Accepted Manuscript

not to the same extent.[45] To account for this effect, we consider different net attachment rates of the Pt atoms on the two orientations, f_0 and f_1 for the {001} and {111} facets, respectively. These net attachment rates are defined as the effective (net) number of Pt atoms attached per unit area, per unit time. Referring to Figure 3, we rationalize the growth of these two facets in terms of these net attachment fluxes. Between times t and $t + dt$, the {001} and {111} facets advance outwards with velocities $V_0 = f_0 / \rho$ and $V_1 = f_1 / \rho$, respectively, where ρ is the number of atoms per unit volume in bulk crystalline Pt (number density). In the absence of a continuous set of surface orientations, the shape at any time t (after the initial instant at which facets form) is given by all the facets that are present at that time. When the net fluxes for various surface orientations are different from one another, their linear in-plane dimensions (represented in Figure 3 by the lengths b_0 and b_1) will also grow at different rates. These linear dimensions can be computed from geometry, assuming that the corners and edges of the NPs are atomically sharp, *i.e.*, only true facets exist forming sharp edges and step bunches are absent. In the quadrilateral ABCD (Figure 3) , we have AB = $b_1(t+dt)$-$b_1(t)$=db_1, BC=V_1dt, CD = $b_0(t)$-$b_0(t+dt)$=-db_0, AD = V_0dt, and the angle between AB and AD measures 90^o-θ, where θ is the angle between the surface normals [001] and [111]. After extending the segment DC until it crosses the line AB at C' (see Figure 3), we can obtain AB (=db_1) as AB=AC' - BC' = $V_0dt/\sin\theta$ -$V_1dt/\tan\theta$; the length CD (=-db_0) can be obtained in a similar manner, leading to expressions of the variations of the lengths b_0 and b_1 per unit time, i.e., the time derivatives of the linear dimensions of the facets.

$$\frac{db_0}{dt} = \frac{V_1 - V_0\cos\theta}{\sin\theta} \qquad \textbf{(1)}$$

$$\frac{db_1}{dt} = \frac{V_0 - V_1\cos\theta}{\sin\theta} \qquad \textbf{(2)}$$

Equations analogous to (1) and (2) can be set up for any two intersecting facets, so that all the corresponding dimensions can be obtained. For the sake of clarity, we limit the discussion to only two facets. From Eqs. (1-2) we note that there are several regimes that can develop during growth, depending on the instantaneous derivatives of b_0 and b_1. For example, both facets can increase in size ($db_0/dt > 0$ and $db_1/dt > 0$) provided that $V_1 > V_0 \cos\theta$ and $V_0 > V_1 \cos\theta$. Interestingly, there is also a regime when $db_0/dt < 0$ and $db_1/dt > 0$, in which the characteristic

Nanoscale Accepted Manuscript

length b_0 of the {001} facet decreases. This is, in fact, the regime depicted qualitatively in Figure 3, which is characterized (refer to Eqs. (1-2)) by $V_1 < V_0 \cos\theta$. In practice, the growth velocities can be time-dependent and can be directed by agents such as $AgNO_3$ that affect the growth rates on the {001} and {111} facets differently.

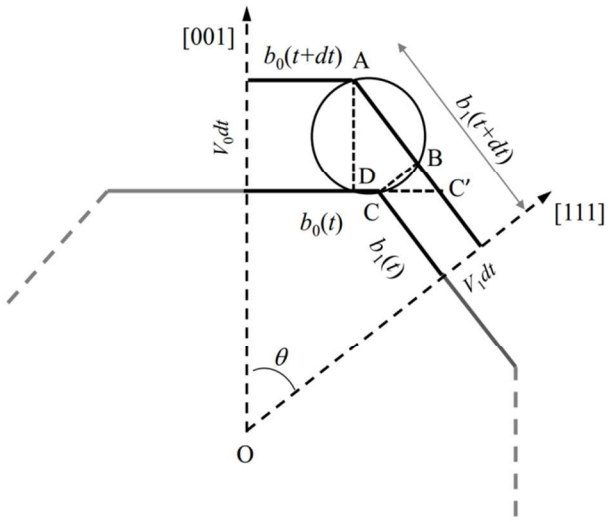

Figure 3. Two intersecting facets growing at different rates V_0 and V_1. Faster growth along [001] direction can lead to a decrease in the linear dimension b_0 of the {001} facet and an increase in the dimension b_1 of the {111} facet.

Explanation of the shape-direction of Pt nanoparticles

As discussed in the previous section, the growth velocities along the [001] and [111] directions are proportional to the net attachment fluxes f_0 and f_1, respectively. If net fluxes f_0 and f_1 are known as functions of time, then Eqs. (1-2) can be integrated to yield the characteristic lengths b_0 and b_1 as functions of time for the entire NP evolution following the moment at which it developed facets. While time-dependent information regarding the fluxes f_0 and f_1 is hard to obtain from first-principles calculations (which are performed usually in vacuum and at zero Kelvin) for conditions that refer specifically to solution synthesis, we can adopt approximate models that capture the main physics of growth. For example, f_1 should decrease to zero fairly rapidly, which is indicative of the Ag "poisoning" of the {111} facets; f_0 should decrease as well, only at a much slower pace than f_1, because the Pt atoms are more abundant in solution and are consumed at a slower rate than silver. We adopt an exponential decay model for the two fluxes, with different time constants τ_0 and τ_1 ($\tau_1 < \tau_0$)

Nanoscale Accepted Manuscript

$$f_{0,1} = C_{0,1} \exp(-t/\tau_{0,1}) \quad \textbf{(3)}$$

where $C_{0,1}$ are the initial values of the two decaying fluxes. With models for net fluxes given by Eq. (3), the integration of Eqs. (1-2) yields:

$$b_0(t) = b_0(0) + \frac{C_1\tau_1(1-\exp(-t/\tau_1)) - C_0\tau_0(1-\exp(-t/\tau_0))\cos\theta}{\rho \sin\theta} \quad \textbf{(4)}$$

$$b_1(t) = b_1(0) + \frac{C_0\tau_0(1-\exp(-t/\tau_0)) - C_1\tau_1(1-\exp(-t/\tau_1))\cos\theta}{\rho \sin\theta} \quad \textbf{(5)}$$

We start with the simple and reasonable assumptions that $b_0(0) = b_1(0)$ (≡B) and $C_0 = C_1$, meaning that initially the characteristic lengths of the two facets are the same, and the net attachment rates to different facets are also the same. Depending on the time constants τ_0 and τ_1, Eqs. (4-5) can predict several types of NP final shapes bound by {001} and/or {111} facets: tetrahedra, truncated tetrahedra, octahedra, and cuboctahedra. For example, when the time constants τ_0 and τ_1 are relatively close to one another, we obtain cuboctahedra as final shapes (Figure 4A). In experiments, control over the fluxes f_1 and f_0 is exercised through the concentration of $AgNO_3$ in solution;. In the case of Pt, Ag may attach to one or both of the {001} and {111} facets, preferentially poisoning only the {111} surface orientation (*i.e.*, effectively blocking the growth along the [111] direction). The regime of lower Ag concentrations in solution is modeled by setting the time constants in Eq. (3) to have similar magnitudes; this leads to the presence of both {111} and {001} facets on the asymptotic shapes (cuboctahedra in Figure 4A and Figure 2B,E). In order to have only {111} facets, we increase the difference between the time constants τ_0 and τ_1 ($\tau_1 << \tau_0$), thus modeling the regime of higher Ag concentration in experiments. As a result, the net flux on the {111} facets decays to near-zero much faster than the net flux f_0 on {001} facets, whose decrease is only due to the consumption/depletion of the Pt atoms from solution due to the growth of the NPs. Indeed, using $\tau_1 = \tau_0 / 20$ in Eqs. (4-5) leads to the disappearance of the {001} facets, and therefore to shapes that are either octahedral or tetrahedral. This case is shown in Figure 4B, where the {001} facets monotonically decrease and vanish altogether past a certain moment, which can be estimated using Eqs. (4-5).

Nanoscale Accepted Manuscript

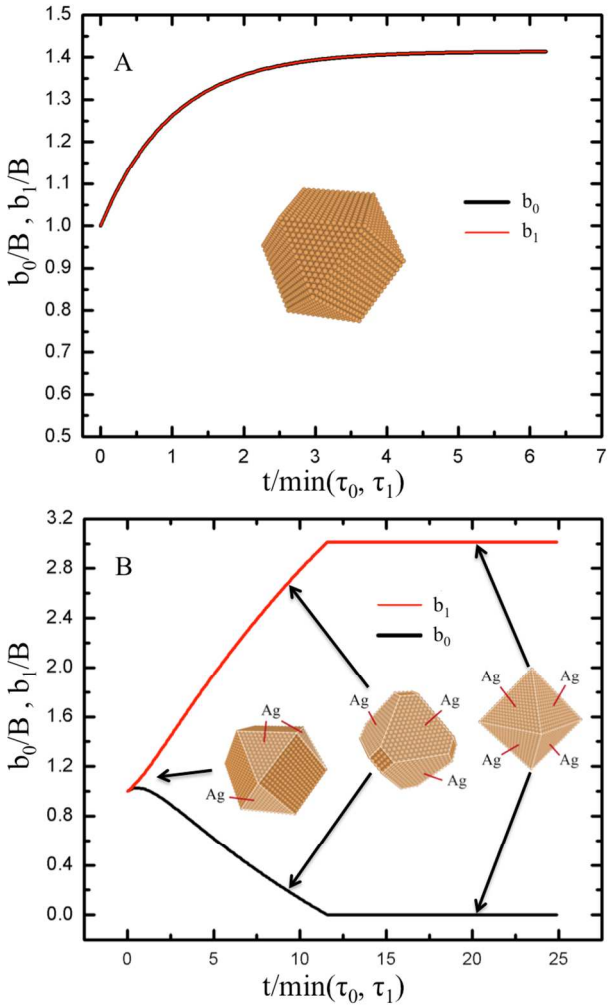

Figure 4. Growth model predictions for the evolution of the characteristic lengths of the {001} and {111} facets in the presence of Ag in solution. (A) For midrange Ag concentration (11 mol%), the time constants controlling the net attachment fluxes are comparable, $\tau_1 = \tau_0$, which leads to the presence of both {001} and {111} facets in the final shapes, *i.e.* cuboctahedra. (B) At higher Ag concentration, (*e.g.* $\tau_1 = \tau_0 / 20$) the {001} facets disappear and the final shape is bounded by {111} facets, *i.e.* octahedra.

Predicting directed growth for Pd NPs

While varying Ag concentration in solution during growth can lead to final NPs with different shapes, the question arises as to what can be done in order to achieve shape-directed NPs using other chemical species and with other metals. Here, we demonstrate the applicability of our growth model to predict the shapes of Pd, a catalytically-important metal that has a face-centered cubic crystal structure with a lattice constant similar to that of Pt. If we grow Pd particles using $AgNO_3$ as the directing agent, then the Ag atoms deposited epitaxially on the Pd facets

Nanoscale Accepted Manuscript

experience compression due to ~5% lattice mismatch. Similar to the case of Pt NPs, Ag atoms are more likely to bind to Pd {111} facets than to {001}, since on the {111} facets are in a close-packed environment that can withstand the compression dictated by the mismatch strain. On the {001} facets, Ag atoms may bind but are unlikely to form epitaxial layers that would withstand compression and block the growth along [001]; the spacing between {001} layers is larger than that between {111} layers, which helps exchanges between Ag and Pd atoms on the {001} facets, and therefore does not inhibit Pd growth along [001]. We therefore expect that growth of Pd NPs can be directed by Ag in solution to produce {111} faceted NPs. This was confirmed by our experiments using the same $AgNO_3$ directed synthesis of Pt outlined in the methods, but changing the precursor salt to K_2PdCl_6. For solutions containing 1 to 5 mol% Ag/Pd, we obtain NPs with primarily {111} facets: octahedral, tetrahedral, and icosahedral morphologies (Figure 5). The model predictions are qualitatively validated by the experimental results. As expected, the kinetics of atom attachment anisotropy are different for Pd and Pt, and hence careful tuning of solution chemistry will be necessary to obtain NPs of a desired shape. Additionally, we carried out synthesis experiments using copper bromide as a directing agent due to copper's chemical similarity to Ag and found that it did not direct the shape of Pt NPs (see supplementary information). This observation suggests that the shape-directing influence of Ag may stem from some other unique property. Corroboration of other experimental systems with this model may have a broader impact for nanomaterial design.

Nanoscale Accepted Manuscript

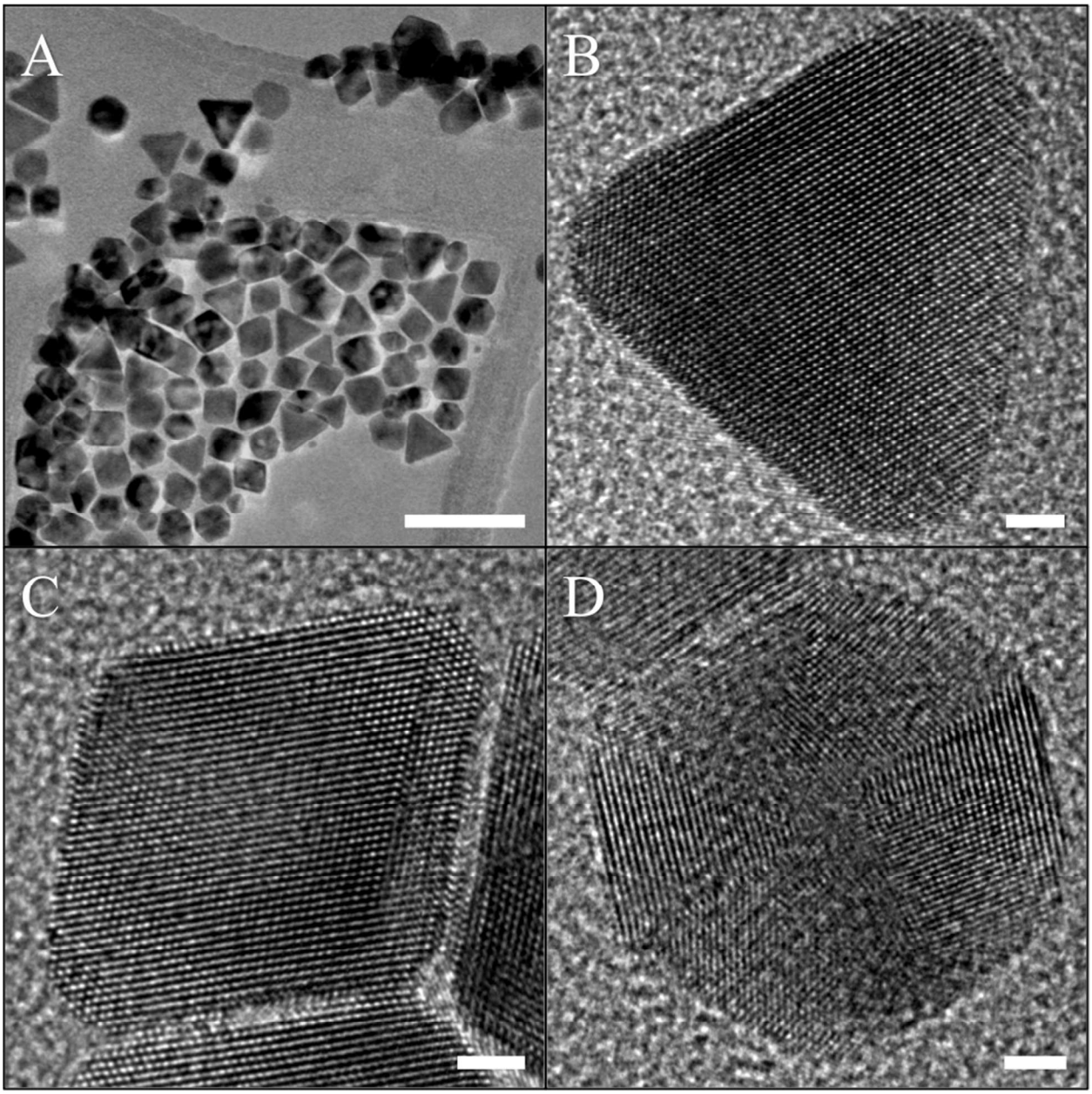

Figure 5. (A) Low magnification TEM and (B-D) HRTEM images of faceted Pd NPs synthesized from K_2PdCl_6 with $AgNO_3$ as a directing agent. {111} surface faceting is predominant in all of the observed NP morphologies: (B) tetrahedral, (C) octahedral, and (D) icosahedral. Scale bars are 50 nm in (A) and 2 nm in (B-D).

Directing Pt Growth by Other Directing Agents

Pt NPs with cubic shapes bounded by {001} facets have been previously demonstrated.[36,54,55] Interestingly, the shape-direction in these experiments was achieved using very diverse directing

Nanoscale Accepted Manuscript

agents (*e.g.* tetradecyltrimethylammonium bromide,[36] $Fe(CO)_5$,[54] and short peptides[55]), all of which lead to cubic or truncated-cubic NPs. The findings can also be explained by our growth model if we assume that the new directing agents restrict the growth along the [001] direction or promote it along the [111] direction. This would be accounted for by relaxation times corresponding to slower growth along [001] than along [111], *i.e.* $\tau_0 < \tau_1$; with this inequality, Eqs. (4 and 5) predict NPs (shown in Figure 6) that are truncated cubes when $\tau_0 < \tau_1$ but are similar order of magnitude, or cubes when $\tau_0 << \tau_1$. While further applications of the model (for example, those involving icosahedral NPs involving twin boundaries) would not be possible without significantly increasing its complexity, its current ability to cover the spectrum from {001} faceted single-crystal NPs to {111} faceted single-crystal NPs unifies a large set of experiments under a simple kinetic model.

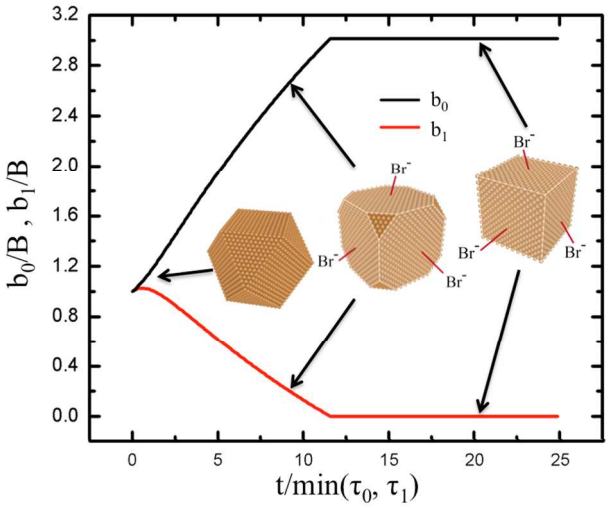

Figure 6. Growth model predictions for the evolution of the characteristic lengths of the {001} and {111} facets in the presence of Br^- in solution. In the presence of Br^-, (*e.g.* $\tau_1 = 20\,\tau_0$) the {111} facets disappear and the final shape is bounded by {001} facets, *i.e.* cube.

Conclusions

By experimentally probing the parameter space influencing nanoparticle shape control, we have developed a model that explains the preferential growth of specific facets. The presence of a shape directing agent (*i.e.* Ag) alters the attachment kinetics of the metal particle (*i.e.* Pt) on {001} and {111} facets, which is reflected in the model in the form of different time constants for the decaying net fluxes to these facets. The model was then employed for another metal (Pd)

Nanoscale Accepted Manuscript

and was able to explain the fluxes associated with the formation of {111} faceted particles. Furthermore, the model also provides a mechanistic explanation for experimental observations reported in the literature,[35,53,54] and can help predict the shape and size of the final NPs. If coupled with models for nucleation,[56] our growth model could lead to a complete computationally-guided design paradigm for shape-directed NPs in which the parameters necessary for achieving a final desired shape and size can be predicted based on solution conditions.

Experimental

Pt NPs with cubic, cuboctahedral, and octahedral shapes were synthesized using a well-known wet chemical reduction procedure.[45] In short, a 2-neck 25 mL round bottom flask was cleaned by soaking in freshly prepared aqua regia overnight followed by rinsing with copious amounts of 18.2 MΩ deionized H_2O before drying in a 100 ˚C forced convection oven. Ethylene glycol (EG, 2.5 mL, Macron Fine Chemicals #5001) was added to the dry flask, the flask fitted with a condenser, and heated to reflux (~200 ˚C). A 0.375 M solution of polyvinylpyrrolidone (PVP, M_w=55,000, Sigma-Aldich #856568), 0.0625 M solution of H_2PtCl_6•$6H_2O$ (Alfa-Aesar #11051) or K_2PdCl_6 (Sigma-Aldrich #334502) along with desired concentrations of $AgNO_3$ (Sigma-Aldrich, #204390) were prepared in EG. All reagents were used as received without further purification.

To the refluxing EG, 0.5 mL of an auxiliary directing agent was added in one single aliquot (as a control experiment, 0.5 ml pure EG was added for undirected growth) prior to the simultaneous addition of 3.0 mL of 0.375 M PVP at a rate of 0.1875 mL/min and 1.5 mL of the 0.0625 M H_2PtCl_6•$6H_20$ (or K_2PdCl_6) in EG was added at a rate of 0.09375 mL/min. After 16 minutes, the additions were stopped and the reaction was refluxed for an additional 5 minutes. The resulting material was allowed to cool to room temperature and centrifuged at 1057 g for 15 minutes to precipitate any unwanted products (*e.g.* AgCl) formed from the various directing agents and precursors. The supernatant was then separated from any precipitate, diluted with 3 times volume of acetone and centrifuged again at 2935 g for 15 minutes to precipitate the Pt nanocrystals into a pellet. The cloudy supernatant was decanted, and the resulting pellet was dispersed in 3 mL ethanol *via* sonication, diluted with 3 times volume of hexanes, and

Nanoscale Accepted Manuscript

centrifuged at 1057 g for 5 minutes to precipitate the Pt nanocrystals into a pellet. Three iterations of the ethanol/hexane cleanings were performed to remove as much excess PVP as possible from the solution. The final products were dispersed and stored in 3 mL ethanol to be drop-cast onto 300-mesh copper TEM grids with either holey or lacey carbon, and were analyzed using a FEI Titan S/TEM operated at 300 kV.

Acknowledgements

This work is funded in part by the Laboratory Directed Research and Development (LDRD) Program at the National Renewable Energy Laboratory, under contract award UGA-0-41025-05. NREL is a national laboratory of the U.S. Department of Energy, Office of Energy Efficiency and Renewable Energy, operated by the Alliance for Sustainable Energy, LLC. GHG and CVC acknowledge support from Lawrence Livermore National Laboratory (Contract B601600). CVC and SK acknowledge support from NSF through Grant No. CMMI-0846858 and CMMI-1200547, respectively.

References

1 G. J. Leong, M. C. Schulze, M. B Strand, D. Maloney, S. L. Frisco, H. N. Dinh, B. Pivovar and R. M. Richards, *Appl. Organomet. Chem.*, 2014, **28**, 1-17.
2 F. Zaera, *ChemSusChem*, 2013, **6**, 1797–1820.
3 K. An, G. A. Somorjai, *ChemCatChem*, 2012, **4**, 1512–1524.
4 H. Zhang, M. Jin, Y. Xiong, B. Lim, Y. Xia, *Acc. Chem. Res.*, 2013, **46**, 1783–1794.
5 F. Zaera, G. A. Somorjai, *J. Am. Chem. Soc.*, 1984, **106**, 2288–2293.
6 A. Wieckowski, S. D. Rosasco, G. N. Salaita, A. Hubbard, B. E. Bent, F. Zaera, D. Godbey, G. A. Somorjai, *J. Am. Chem. Soc.*, 1985, **107**, 5910–5920.
7 N. Markovic, H. Gasteiger, P. N. Ross, *J. Electrochem. Soc.*, 1997, **144**, 1591–1597.
8 F. Zaera, *Langmuir*, 1991, **7**, 1998–1999.
9 J. Chen, B. Lim, E. P. Lee, Y. Xia, *Nano Today*, 2009, **4**, 81–95.
10 J. Horáček, G. Šťávová, V. Kelbichová, D. Kubička, *Catal. Today*, 2013, **204**, 38–45.
11 O. Långvik, P. Mäki-Arvela, A. Aho, T. Saloranta, D. Y. Murzin, R. Leino, *Catal. Lett.*, 2013, **143**, 142–149.
12 K. M. Bratlie, H. Lee, K. Komvopoulos, P. Yang, G. A. Somorjai, *Nano Lett.*, 2007, **7**, 3097–3101.
13 I. Lee, F. Zaera, *Top. Catal.*, 2013, **56**, 1284–1298.
14 A. Fukuoka, J.-I. Kimura, T. Oshio, Y. Sakamoto, M. Ichikawa, *J. Am. Chem. Soc.*, 2007, **129**, 10120–10125.
15 J. N. Kuhn, C.-K. Tsung, W. Huang, G. A. Somorjai, *J. Catal.*, 2009, **265**, 209–215.
16 R. Jensen, T. Andersen, A. Nierhoff, T. Pedersen, O. Hansen, S. Dahl, I. Chorkendorff, *Phys. Chem. Chem. Phys.*, 2013, **15**, 2698–2702.
17 Z.-Y. Zhou, Z.-Z. Huang, D.-J. Chen, Q. Wang, N. Tian, S.-G. Sun, *Angew. Chem., Int. Ed.*, 2010, **49**, 411–414.
18 H. Bönnemann, G. Khelashvili, *Appl. Organomet. Chem.*, 2010, **24**, 257–268.
19 M. Shao, A. Peles, K. Shoemaker, *Nano Lett.*, 2013, **11**, 3714–3719.
20 R. Wang, H. He, J. Wang, L. Liu, H. Dai, *Catal. Today*, 2013, **201**, 68–78.
21 S. Kondo, M. Nakamura, N. Maki, N. Hoshi, *J. Phys. Chem. C*, 2009, **113**, 12625–12628.
22 M. Crespo-Quesada, J.-M. Andanson, A. Yarulin, B. Lim, Y. Xia, L. Kiwi-Minsker, *Langmuir*, 2011, **27**, 7909–7916.

Nanoscale Accepted Manuscript

23 M. Crespo-Quesada, A. Yarulin, M. Jin, Y. Xia, L. Kiwi-Minsker, *J. Am. Chem. Soc.*, 2011, **133**, 12787–12794.
24 Y.-F. He, J.-T. Feng, Y.-Y. Du, D.-Q. Li, *ACS Catal.*, 2012, **2**, 1703–1710.
25 J. Turkevich, G. Kim, *Science*, 1970, **169**, 873–879.
26 M. Shao, T. Yu, J. H. Odell, M. Jin, Y. Xia, *Chem. Commun.*, 2011, **47**, 6566–6568.
27 Y. Li, X. M. Hong, D. M. Collard, M. A. El-Sayed, *Org. Lett.*, 2000, **2**, 2385–2388.
28 Y.-T. Chu, K. Chanda, P.-H. Lin, M. H. Huang, *Langmuir*, 2012, **28**, 11258–11264.
29 S.-W. Kim, M. Kim, W. Y. Lee, T. Hyeon, *J. Am. Chem. Soc.*, 2002, **124**, 7642–7643.
30 M. T. Reetz, E. Westermann, *Angew. Chem., Int. Ed.*, 2000, **39**, 165–168.
31 A. R. Tao, S. Habas, P. Yang, *Small*, 2008, **4**, 310–325.
32 C. M. Sánchez-Sánchez, J. Solla-Gullón, F. J. Vidal-Iglesias, A. Aldaz, V. Montiel, E. Herrero, *J. Am. Chem. Soc.*, 2010, **132**, 5622–5624.
33 R. Narayanan, M. A. El-Sayed, *Nano Lett.*, 2004, **4**, 1343–1348.
34 H. A. Gasteiger, N. M. Markovic, *Science*, 2009, **324**, 48–49.
35 I. Lee, F. Delbecq, R. Morales, M. A. Albiter, F. Zaera, *Nat. Mater.*, 2009, **8**, 132–138.
36 H. Lee, S. E. Habas, S. Kweskin, D. Butcher, G. A. Somorjai, P. Yang, *Angew. Chem.*, 2006, **118**, 7988–7992.
37 X. Gong, Y. Yang, L. Zhang, C. Zou, P. Cai, G. Chen, S. Hunag, *J. Colloid Interface Sci.*, 2010, **352**, 379–385.
38 H. Wang, H. Y. Jeong, M. Imura, L. Wang, L. Radhakrishnan, N. Fujita, T. Castle, O. Terasaki, Y. Yamauchi, *J. Am. Chem. Soc.*, 2011, **133**, 14526–14529.
39 H. Wang, M. Imura, Y. Nemoto, S.-E. Park, Y. Yamauchi, *Chem. – Asian J.*, 2012, **7**, 802–808.
40 C. Li, M. Imura, Y. Yamauchi, *Phys. Chem. Chem. Phys.*, 2014, **16**, 8787-8790.
41 C. Li, Y. Yamauchi, *Phys. Chem. Chem. Phys.*, 2013, **15**, 3490–3496.
42 B. Lim, H. Kobayashi, P. H. C. Camargo, L. F. Allard, J. Liu, Y. Xia, *Nano Res.*, 2010, **3**, 180–188.
43 Y. Xia, Y. Xiong, B. Lim, S. E. Skrabalak, *Angew. Chem., Int. Ed.*, 2009, **48**, 60–103.
44 S. Curtarolo, G. L. W. Hart, M. B. Nardelli, N. Mingo, S. Sanvito, O. Levy, *Nat. Mater.*, 2013, **12**, 191–201.
45 H. Song, F. Kim, S. Connor, G. A. Somorjai, P. Yang, *J. Phys. Chem. B*, 2005, **109**, 188–193.
46 M. E. Grass, Y. Yue, S. E. Habas, R. M. Rioux, C. I. Teall, P. Yang, G. A. Somorjai, *J. Phys. Chem. C*, 2008, **112**, 4797–4804.
47 T. Herricks, J. Chen, Y. Xia, *Nano Lett.*, 2004, **4**, 2367–2371.
48 B. Soroushian, I. Lampre, J. Belloni, M. Mostafavi, *Radiat. Phys. Chem.*, 2005, ***72***, 111–118.
49 G. Z. Wulff, *Z. Kristallogr. Mineral.*, 1901, **34**, 449–530.
50 V. Shenoy, *Phys. Rev. B*, 2005, **71**, 094104.
51 W.-B. Zhang, C. Chen, S.-Y. Zhang, *J. Phys. Chem. C*, 2013, **117**, 21274–21280.
52 D. Yu, H. Bonzel, M. Scheffler, *Phys. Rev. B*, 2006, **74**, 115408.
53 A. Pimpinelli, J. Villain, in *Physics of Crystal Growth (Collection Alea-Saclay: Monographs and Texts in Statistical Physics)*, Cambridge University Press, New York, 1998, ch. 4, pp. 60–69.
54 C. Wang, H. Daimon, T. Onodera, T. Koda, S. Sun, *Angew. Chem., Int. Ed.*, 2008, **47**, 3588–3591.
55 L. M. Forbes, A. P. Goodwin, J. N. Cha, *Chem. Mater.*, 2010, **22**, 6524–6528.
56 V. K. LaMer, R. G. Dinegar, *J. Am. Chem. Soc.*, 1950, **72**, 4847–4854.

Nanoscale Accepted Manuscript